Classification: Biological Sciences – Computational Biology

Title: Computational redesign reveals allosteric mutation hotspots of organophosphate hydrolase that enhance organophosphate hydrolysis

Reed B. Jacob[a], Feng Ding[b], Dongmei Ye[c], Eric Ackerman[c], and Nikolay V. Dokholyan[a]

[a] Department of Biochemistry and Biophysics, University of North Carolina Chapel Hill, 120 Mason Farm Rd, Campus Box 7260, 3rd Floor, Genetic Medicine Building, Chapel Hill, NC 27599
[b] Department of Physics and Astronomy, Clemson University, Clemson, SC 29634
[c] Sandia National Laboratories, 1515 Eubank SE, Albuquerque, NM 87123

Corresponding author: Nikolay V. Dokholyan, 120 Mason Farm Rd, Campus Box 7260, Genetic Medicine Building, Chapel Hill, NC 27599, 919-843-2513, dokh@unc.edu

Keywords: protein design, organophosphate hydrolase, organophosphates

Abstract

Organophosphates are widely used for peaceful (agriculture) and military purposes (chemical warfare agents). The extraordinary toxicity of organophosphates and the risk of deployment, make it critical to develop means for their rapid and efficient deactivation. Organophosphate hydrolase (OPH) already plays an important role in organophosphate remediation, but is insufficient for therapeutic or prophylactic purposes primarily due to low substrate affinity. Current efforts focus on directly modifying the active site to differentiate substrate specificity and increase catalytic activity. Here, we present a novel strategy for enhancing the general catalytic efficiency of OPH through computational redesign of the residues that are allosterically coupled to the active site and validated our design by mutagenesis. Specifically, we identify five such hot-spot residues for allosteric regulation and assay these mutants for hydrolysis activity against paraoxon, a chemical-weapons simulant. A high percentage of the predicted mutants exhibit enhanced activity over wild-type (k_{cat} =16.63 s^{-1}), such as T199I/T54I (899.5 s^{-1}) and C227V/T199I/T54I (848 s^{-1}), while the K_m remains relatively unchanged in our high-throughput cell-free expression system. Further computational studies of protein dynamics reveal four distinct distal regions coupled to the active site that display significant changes in conformation dynamics upon these identified mutations. These results validate a computational design method that is both efficient and easily adapted as a general procedure for enzymatic enhancement.

Significance Statement

Enzymes are one of nature's basic building blocks and hold the key to protecting armed forces and civilians against chemical weapons of mass destruction. Weaponized organophosphates are a deadly threat (*i.e.* exposure to one droplet of VX exceeds the LD_{50} of ~15 μg/kg) we have little protection against. Organophosphate hydrolase (OPH) degrades many classes of organophosphates and plays an important role in organophosphate remediation. Here we propose a computational protein design strategy to inform mutation of OPH to enhance enzymatic hydrolysis of paraoxon. We have discovered five residue positions allosterically effecting enzymatic activity and temperature stability. By increasing the activity of OPH nearly two orders of magnitude, we validated this unique approach representing a shift in focus from direct active site manipulation to alteration of residues associated with allosteric involvement in enzyme activity.

Introduction

Organophosphates prevent acetylcholinesterase from clearing the neurotransmitter acetylcholine, blocking key signals of the central nervous system leading to asphyxiation and death (1). Shortly after discovery, organophosphates were formulated for use as chemical weapons, rapidly rising to great prominence as weapons of mass destruction (i.e. recent Syrian attack with sarin gas, August 2013). The existing vulnerability due to limited protective measures is of great concern and has spurred investigations into the enzymatic hydrolysis of organophosphates for remedial and therapeutic use. The currently used enzyme for remediation is organophosphate hydrolase (OPH) (2), which is a bi-metallo-coordinated enzyme existing naturally as a homodimer, where each subunit contains two zinc ions coordinated to form the binding site (Figure 1a). An ideal

enzyme engineered for remediation would be capable of degrading multiple organophosphate nerve agents. OPH has effect against most nerve agents with various hydrolysis rates of a k_{cat} of 0.30 s^{-1} for V-agent VX and 56 s^{-1} for G-agent sarin (3, 4). The known simulant closest to native activity is paraoxon with a k_{cat} of 2400 s^{-1} (5).

The majority of investigative efforts focus on modifying the specificity of OPH for various nerve agents through either random mutagenesis or rational design, directed evolution and computationally directed evolution, concentrating on mutations to the active site surrounding the zinc ions (6–8). While promising, these efforts detract from the generalizability of OPH for multiple nerve agents. In our work, we broaden the scope of investigation to encompass interior residues with potential allosteric interactions that increase general enzymatic activity as assayed by paraoxon. We show an increase in the hydrolysis rates of paraoxon with both single and multiple mutations and anticipate an increase for all organophosphate nerve agents. In addition, we expect that our approach is orthogonal to other engineering methods near the active site and our mutations can be combined with previously designed OPH variants for further enhancement.

Our design method relies on computational stability prediction of enzyme in the active state combined with experimental validation and computational analysis through equilibrium discrete molecular dynamics (DMD), and replica exchange DMD. When applying this method to OPH, we identified five residue positions located between five and ten Å from the active site, mutations with which increased paraoxon activity more than 50-fold experimentally. Next we demonstrate a general workflow designed to enhance native enzymatic activity.

Results

Prediction and experimental validation of single mutations. Crucial to any enzyme design strategy is the identification of key residues, that when mutated, correctly modify the protein in the desired manner. The methods behind selecting these residues vary from experimental techniques such as alanine scanning, to more computationally expensive methods such as transition state modeling (9, 10). The majority of these methods concentrate only on the active site itself, while few of them probe potential allosteric modifications. Methods that utilize protein allostery are computationally intensive, such as the molecular mechanics-generalized born surface area with molecular dynamics method described by Sirin et al (11). Here we present a method to predict key residue positions that is both quick and efficient while maintaining a generality that can be applied across the entire protein. Central to this protocol is our protein stability prediction algorithm, Eris (12, 13). With the knowledge of the native state structure, Eris estimates the changes in protein stability by calculating $\Delta\Delta G$, the free energy difference between the folded and unfolded states after mutations. Because an enzyme is highly dynamic in solution with the catalytically active state constituting a fraction of the native state ensemble and the stability of a given state determines its relative population, we hypothesize that mutations stabilizing the catalytically-active state increase the probability of the enzyme to sample its active form, enhancing the catalysis reaction. Based on high-resolution structure of an enzyme in its active state, we can identify these hotspot residues by estimating $\Delta\Delta G$ values of all possible single- or multiple-mutations of residues away from the active states.

We applied this protocol to OPH to find mutations that increase enzymatic activity (Methods and Figure 1b). The results from scanning OPH for single-mutations indicated five

mutations that significantly (*Z*-score < -3) increase stability: T54M, D105T, T199I, C227M, and G251L with ΔΔG scores of -5.0, -6.7, -8.1, -3.8, and -6.7 kcal/mol respectively (Table 1). Examination of the wild-type crystal structure reveals that these residues are either near an internal void formed by residues T54, T199, C227 and G251, or corresponding to a buried and unpaired charge, D105 (Figure 1c-d). The stabilization effect is either due to increases of the side chain volume to fill the cavity or to reduce the desolvation penalty of buried charges.

To assess the utility and accuracy of our computational methods we tested our predictions experimentally. Wild-type and mutant OPH were expressed in a wheat-germ cell free system. To establish the validity of our expression system, and the effect it has on OPH, we compared the activity of cell-free generated wild-type OPH, with a k_{cat} of 16.63 s^{-1} under cell lysate conditions, to identically expressed mutants. The wild-type activity in lysates is slower compared to pure wild-type OPH run in standard conditions, k_{cat} of 1997.0 s^{-1}. To verify that the cell lysate machinery inhibits purified OPH, we spiked our cell free system cell lysate machinery with pure wild-type OPH and observed ~120-fold reduction in paraoxon activity (data not shown). Expecting that the inhibitory effects are the same for both wild-type and mutant OPH, we performed all assays in the expression environment of the cell lysate machinery and compared the paraoxon hydrolysis activities of all predicted mutations with that of the wild-type under the same cell-free condition.

The OPH mutations T199I, C227M, and T54M each showed measurable catalysis kinetics with k_{cat} values of 487.9, 33.05, and 9.804 s^{-1} respectively (Table 1). Mutants G251L and D105T expressed but showed no apparent activity. Compared to the wild-type OPH k_{cat} of 16.63 s^{-1}, the T199I mutation increases the k_{cat} by 3000% while the C227M mutation only increases k_{cat} by 200%. The OPH T54M mutant shows no increase in k_{cat}. The K_m changes no more than 27% among any of the three mutants.

Prediction of double and triple mutations with experimental validations. With the experimentally identified three hot-spot residues—T54, T199 and C227, we therefore extended our ΔΔG calculation for all possible double and triple mutations. Based on Eris calculations, we identified following stabilizing double-mutants: T54I/T199I, T54M/T199I, T54I/C227M, T54I/C227V, T54M/C227M, T199I/C227M, and T199I/C227V; and triple-mutants: T54I/T199I/C227M, T54I/T199I/C227V, and T54M/T199I/C227M (Table 1). We note that the stabilizing double- and triple-mutations are not simple combination of the stabilizing single-mutations, which is due to the coupling of these residues. For example, T54I was not as stabilizing as T54M in single mutations but becomes more stabilizing when combined with other mutations. The same observation is true for C227V. The most successful combinations included those with T199I. For example, T199I alone has a predicted ΔΔG of -8.1 kcal/mol, but when combined with C227M and C227V the predicted score improved to -10.3 kcal/mol and -9.8 kcal/mol respectively. Additionally, when T199I is combined with T54I the improved stability increased to a total predicted score for the double mutation T199I/T54I of -12.5 kcal/mol (Table 1).

We also tested these double and triple mutations experimentally. Interestingly, we found that double and triple mutants containing T54M showed low expression compared to those containing T54I. We also discovered that replacing the C227M mutation with C227V improved expression of double and triple mutants. The C227M/T199I and C227M/T54M mutations increased k_{cat} 2000% and 400% respectively. The T199I/T54M mutant did not express, but the

mutant T199I/T54I increased activity by over 5000% with a k_{cat} of 899.5 s^{-1} (Figures 2a and S1). Compared to multi-mutants with C227M, the mutations replaced with C227V had little effect on the double mutants, but in the C227V/T199I/T54I triple mutant the mutation increased the k_{cat} to 848.1 s^{-1} compared to 781.2 s^{-1} from the C227M/T199I/T54I mutant.

Mutant activities at high temperatures. Enzymes for organophosphate remediation under combat conditions are required to function at elevated temperatures. We tested the activity level of the OPH mutants at both 50°C and 60°C. Aliquots of protein were sampled after 0, 15, 30, 60, 120, 180, and 240 minutes exposure to increased temperatures and assayed for paraoxon hydrolysis (Figures 2b-c and S2). Mutation T199I improves specific activity over wild-type for the first thirty minutes at 50°C with an increase from wild-type OPH of 7.3 to 40.7 U/mg. Though beyond thirty minutes T199I quickly falls below the level of activity of wild-type OPH. Similarly, T199I shows an initial tenfold increase in activity at 60°C for 15 minutes and falling below wild-type activity thereafter. The other single mutations didn't significantly increase activity over wild-type OPH, but mutant T54M maintained its level of activity for the full 240 minutes.

For double mutants, the addition of mutation T54I increases the activity of mutant T199I/T54I to approximately seventy fold that of wild-type for over 240 minutes as compared to the single T199I mutation for 30 minutes at 50°C. At 60°C, T199I/T54I activity is increased by thirty fold at 15 minutes, but maintains improved performance over wild-type OPH for over 30 minutes, extending the activity intensity and duration of single mutant T199I. All other double mutants increased initial activity from twofold (C227M/T54M) to fourteen fold (C229M/T199I) at both 50°C and 60°C (Figure S2).

When considering the triple mutations, both C227M/T199I/T54I and C227V/T199I/T54I show an improved activity of 60.5 U/mg and 69.2 U/mg, respectively, over wild-type OPH of 3.3 U/mg. This improved activity at 50°C is lost by sixty minutes for C227M/T199I/T54I, whereas C227V/T199I/T54I maintains enriched activity until the 120 minutes sample. Similarly, at 60°C, the enhanced activity of C227M/T199I/T54I is lost by fifteen minutes, where triple mutant C227V/T199I/T54I maintains activity till thirty minutes.

Computational analysis of thermostability and conformational dynamics. To improve future design endeavors, it is important to fully comprehend the effects a mutation has on a protein. Usually, a mutation can affect the thermo-stability of the entire protein by changing the melting temperature, T_m. Additionally, the proposed mutations would impact the active site through allosteric coupling (14–16). Hence, we computationally investigated our predicted and experimentally validated single, double and triple OPH mutations for both thermal stability and altered active site dynamics. Our first computational analysis examined the effect of OPH mutations on protein stability using replica exchange DMD combined with the weighted histogram analysis method to calculate the specific heat (C_v) (17, 18). The computed C_v plot allowed us to extrapolate an estimated T_m by identifying the temperature at which the specific heat reaches its maximum value. An increase in T_m indicates an increase in thermal stability. Single mutations T199I, C227M, and T54M have a similar T_m, varying from wild-type by ± 2 K (Figures 3a and S3, Table S1). In addition though G251L has a similar T_m, it, like D105T, disrupts the major transition peak creating multiple states that are non-functioning (Figure S3). The C227V/T199I double mutant is stabilizing with an increase in T_m of 2.515 K over wild-type OPH. The remaining double mutants are slightly destabilizing with a ΔT_m ranging from -5.03 to -

10.06 K. Both triple mutants C227M/T199I/T54I and C227V/T199I/T54I are destabilizing with the same T_m of 329.375 K as compared to wild-type of 334.375 K (Table S1 and Figure S3). Through comparing the OPH mutants to the wild-type OPH we establish that the predicted mutations do not have significant impact on the thermal stabilities with slight changes in T_m.

Without significant changes in stability, we examined conformational dynamics of OPH wild-type and mutants. In scrutiny of this explanation, we ran 10 independent DMD simulations with randomized initial velocities for each mutant at a temperature of ~311 K. This temperature was chosen as it is ~10 K lower than the T_m of the least stabilized mutation, C227M/T199I (Table S1). We performed these simulations to identify changes in residue fluctuations between wild-type and mutant OPH by calculating the RMSF for each of the 10 trajectories and averaging them. We used a tube representation of protein structures, where the backbone trace radii are rescaled according to fluctuations and colored from stable (blue) to highly varying (red), to illustrate changes in fluctuations upon mutations (Figure 3b). Our analysis revealed four segments — residues 80-90, 207-224, 261-276, and 311-323 — that represents a significant (p-value < 0.05) change in RMSF (Table 2).

Further, comparing the behavior of these segments across the OPH mutations, the second segment is significantly (p-values < 0.01) rigidified by all mutations with ΔRMSF ranging from -2.93 Å for mutation T199I/T54I to -7.29 Å for mutation C227V/T199I/T54I. Whereas in the first segment the majority of mutations result in increased flexibility compared to the wild-type; such as 227M/T54M (+2.00 Å), C227V/T199I (+3.01 Å), T199I/T54I (+2.58 Å), and C227M/T199I/T54I (+2.47 Å) (Table 2). The one exception is T54M, which significantly rigidified the first segment, ΔRMSF = -2.70 Å. Note that single mutant T54M has a reduced K_{cat} compared to wild-type. Both of the remaining segments show somewhat increased flexibility from many of the mutations with segment three having a ΔRMSF range from 2.01 Å (C227M/T199I) to 4.20 Å (C227V/T199I/T54I) and segment four ranging from 1.53 Å (C227M/T199I) to 3.08 Å (C227V/T199I/T54I). Figure 3b shows the average RMSF of wild-type OPH with the best performing single mutant T199I (red), double mutant T199I/T54I (blue), and triple mutant C227V/T199I/T54I (green).

Discussion

Organophosphates present a credible threat ever since their first appearance in the arena of chemical weapons. The limited effectiveness of current countermeasures has spurred many investigative efforts with the majority of rational redesign targeting active-site modification of known organophosphate hydrolyzing enzymes, such as OPH. To further improve the activity of OPH and its variants, we seek an orthogonal approach to enhance general enzymatic activity by investigating OPH mutations with an allosteric effect on the active site. For this purpose we have created a general workflow that can be applied to any enzyme or protein. This workflow's central component is our protein stability prediction algorithm, Eris. Currently, only one other reported technique probes allosteric mutations, and it is computationally intensive requiring both molecular mechanics and molecular dynamics combined with docking efforts (11). Whereas our algorithm, Eris, calculates the ΔΔG via side-chain repacking and energy minimization making it computationally efficient and can easily scan a residue position in minutes (12, 13).

Using Eris, we targeted interior amino acids away from the active site and obtained five suggested mutations, T199I, T54M, C227M, G251L, and D105T. When expressed experimentally three of the mutations, T199I, T54M, and C227M showed measureable kinetic rates. In contrast, mutations G251L and D105T presented no measureable activity. When G251L and D105T mutations were examined computationally by replica exchange DMD, the C_v-reaction coordinate showed a disruption of the transition temperature peak into many multiple peaks (Figure S3). This disruption suggests that mutations G251L and D105T may have a negative impact, potentially fracturing the protein creating various conformational modes. Visual inspection of the mutated structure reveals a direct effect on metal ion coordinating residues. Because of the lack of activity, mutations G251L and D105T were not considered for experimental validation in the double and triple mutations. This analysis suggests that thermal stability study using DMD may further improve the success rate of Eris prediction of hot-spot residues for experimental validation.

Though none of the tested activity-enhancing mutations affect thermal stability significantly, they do affect the specific activity levels at increased temperature. The assays performed at both 50°C and 60°C show that single mutation T199I improves activity compared to wild-type by 13 fold, but falls below that of wild-type after 30 minutes at 50°C and within 15 minutes at 60°C. Interestingly, mutation at position T54 to either T54M or T54I increases the endurance time. The single T54M mutant maintains a constant level of activity for the entire 240 min at 50°C and for over 60 minutes at 60°C. When combined with T199I, the double mutant T199I/T54I dramatically (70-fold) increases activity over wild-type for the entire duration of 240 minutes at 50°C and over 30 minutes at 60°C (Figures 2 and S2).

The computational investigation revealed that the activity enhancement of the single, double, and triple mutations is due to allosteric effect on the active site. Our RMSF analysis of both wild-type and mutant OPH variants indicated that residue segments 80-90, 207-224, 261-276, and 311-323 are dynamically coupled to the mutation sites. Correlation with the catalytic activities of various mutations suggested that concerted dynamics of whole protein are important for the catalytic function and that rigidification of segment 2 and increased flexibility of other segments are related to the enhancement of catalytic activity (Fig. 3).

In summary, we have described a generalizable approach to enzyme enhancement that focuses on allosteric mutations away from the active sites. The approach depends on rapid screening of hotspot residues using structure-based stability prediction tool, Eris. The central hypothesis is that increasing the stability of the catalytically-active state of an enzyme may increase the population of this state and thus enhance the activity. Experimental characterizations combined with additional computational analysis using DMD simulation suggested that thermo-stability estimation may further improve the prediction accuracy. Further dynamics analysis confirmed the allosteric effect of our proposed mutations and revealed the coupled dynamics important for the catalytic activity of OPH. In total, this work adds a new dimension to the field of protein design through our developed tool of protein stability prediction that we used to enhance the catalytic activity of organophosphate hydrolase increasing the k_{cat} of wild-type OPH up to 5000%. Since the proposed allosteric mutations are away from the catalytic sites, we expect our approach can be combined with other active-site-oriented methods to maximally enhance the activity of OPH.

Methods

Protein stability prediction. Using our in-house developed protein stability algorithm, Eris, we identify mutations that stabilize OPH. The stability of the protein is quantified by the change in free energy (ΔΔG) between the wild-type protein and its mutant. Using the high-resolution dimer structure of OPH (PDB ID: 1DPM), we excluded the residues coordinating zinc and in contact with the substrate. We also exclude the surface residues to reduce possible interruption of protein-protein interaction of OPH. The mutated residues included 53-56, 58, 59, 61-67, 72, 73, 79, 82, 83, 86, 87, 90, 98-105, 107-110, 112, 113, 116, 124-135, 139, 150, 153, 167-172, 175-181, 183, 184, 198-202, 204-212, 215, 216, 227-235, 239, 240, 243, 250-263, 265-270, 273-278, 280, 281, 297-300, 304-307, 309-316, 318-329, and 331-332. For each residue, the native amino acid was mutated to other 19 types. For each sequence (wild type and mutants), we performed 100 independent Monte-Carlo-based protein side-chain repacking using Dunbrack rotamer library (19) and all energy calculations utilize the MedusaScore scoring function (20). With these 100 independent Medusa runs, we computed the average stability $<\Delta G>$ and its standard deviation $\delta(\Delta G)$. For a given mutation, the average ΔΔG is obtained by subtracting the wild-type stability, $<\Delta G>_{mut}-<\Delta G>_{wt}$. The corresponding Z-score is obtained as $\Delta\Delta G/[\delta(\Delta G)_{mut}+\delta(\Delta G)_{wt}]$. Our scanning study suggested that the majority of the positions does not have a strong stabilizing mutations and only a few hotspots can be mutated to increase the stability with significant z-scores ($z < -1.5$).

Site-directed mutagenesis. Site-directed mutagenesis was performed using Quikchange II kit from Agilent. Primers are designed according to manufacturer's protocol and purchased from IDT. 50 μl of PCR reaction containing 5 μl of 10x reaction buffer, 1 μl dNTP mix, and 1.25 μl of each forward and reverse primers, 1 μl pfu ultra polymerase, and 10 ng DNA template was used for mutagenesis reaction. The PCR cycles were: 95 °C, 2 min, 30 cycles of 95 °C, 1 min, 55 °C, 1 min and 72 °C, 1.5 min, followed by 72 °C, 10 min. The resulted PCR products are DpnI digested and then transformed into XL1-blue supercompetent cells.

Plasmid preparation. Plasmids are prepared using Invitrogen maxiprep kit. Sequences were confirmed by Eurofin operon. Plasmid concentrations are determined using nanodrop and adjusted to 1 μg/μl.

Cell-free protein synthesis. Wheat germ cell-free protein synthesis system from Cell-Free Science was used to generate WT and mutant OPH. 20 μl of transcription reactions containing 4 μl of 5x transcription buffer, 2 μl of NTP mix, 0.25 μl of RNase inhibitor, 0.25 μl of SP6 RNA polymerase, 2 μl of plasmid are prepared and incubated at 37 °C for 6 h, then translation reactions containing 10 μl of transcription reaction, 0.8 μl of creatine kinase (1mg/ml), 10 μl of WEPRO, 75 μM of $Zn(OAc)_2$ and 206 μl of SUB-MIX were prepared and incubated at 15 °C for 20 h. The resulting proteins were used for activity assay.

Determination of OPH concentration. Series dilutions of purified recombinant OPH were used as standards. Cell-free generated OPH and standards are loaded to a SDS gel, and OPH concentrations were determined by densitometry using Gel Doc.

*OPH activity assay***.** BioTek plate reader was used for OPH activity assay. Assay condition: 4.3 μl of 46.5 mM paraoxon was added to 193.7 μl of buffer containing 100 mM CHES and 75 μM of $Zn(OAc)_2$, PH = 9.0, reactions were started by adding 2 μl of cell free generated WT or mutant OPH. Activity was then determined by plate reader at 405 nm.

Computational Analysis. All-atom discrete molecular dynamics (DMD) simulations were used to study both thermodynamic properties and the conformational dynamics of OPH. Specifically, we performed replica exchange DMD simulations with 52 replicas ranging from 0.50 to 0.70 kcal/mol/k_B incrementally by 0.004 kcal/mol/k_B. Each simulation was run for $1x10^6$ DMD time steps with a temperature exchange every 1,000 DMD time steps. Each DMD time step corresponds to ~50 fs, and the total simulation time of each replica was ~50 ns. We then applied the weighted histogram analysis method to calculate the specific heat as a function of temperature (21), which was further used to determine the thermal stability of the mutants with respect to the wild-type protein.

Constant temperature equilibrium simulations of OPH and mutants were performed at 0.62 kcal/mol/k_B; this temperature is well below the folding transition temperature (Figures 3, S3 and S4). To identify any major motion deviations we computed an average of the root mean square fluctuations (RMSF) per residue. We performed ten independent simulations for each mutation and wild-type. From each independent trajectory we considered only the time points after the protein reached equilibrium, ~300,000 time steps. The RMSF per residue was calculated using analysis tool g_rmsf from Gromacs (22, 23) then averaged to obtain the final RMSF for comparisons.

Acknowledgements

We thank David Mowrey and Marino Convertino for comments and suggestions on the manuscript. Financial support of DTRA grants HDTRA-1-12-C-0074 to NVD and DTRA100279157 to EJA is gratefully acknowledged. Sandia is a multiprogram laboratory operated by Sandia Corporation, a Lockheed Martin Company, for the U.S. Department of Energy's National Nuclear Security Administration un- der Contract No. DE-AC04-94AL8500.

References

1. Petroianu GA (2010) History of organophosphate synthesis: the very early days. *Pharmazie* 65:306–11.
2. Cho T-H, Wild JR, Donnelly KC (2000) Utility of organophosphorus hydrolase for the remediation of mutagenicity of methyl parathion. *Environ Toxicol Chem* 19:2022–2028.
3. Kanugula AK et al. (2011) Immobilization of organophosphate hydrolase on biocompatible gelatin pads and its use in removal of organophosphate compounds and nerve agents. *Indian J Biochem Biophys* 48:29–34.
4. Grimsley JK, Calamini B, Wild JR, Mesecar AD (2005) Structural and mutational studies of organophosphorus hydrolase reveal a cryptic and functional allosteric-binding site. *Arch Biochem Biophys* 442:169–79.

5. Wong K-Y, Gao J (2007) The reaction mechanism of paraoxon hydrolysis by phosphotriesterase from combined QM/MM simulations. *Biochemistry* 46:13352–69.
6. Di Sioudi BD, Miller CE, Lai K, Grimsley JK, Wild JR (1999) Rational design of organophosphorus hydrolase for altered substrate specificities. *Chem Biol Interact* 119-120:211–23.
7. Bigley AN, Xu C, Henderson TJ, Harvey SP, Raushel FM (2013) Enzymatic neutralization of the chemical warfare agent VX: evolution of phosphotriesterase for phosphorothiolate hydrolysis. *J Am Chem Soc* 135:10426–32.
8. Cherny I et al. (2013) Engineering V-Type Nerve Agents Detoxifying Enzymes Using Computationally Focused Libraries. *ACS Chem Biol* 8:2394–2403.
9. Waldo GL et al. (2010) Kinetic scaffolding mediated by a phospholipase C-beta and Gq signaling complex. *Science* 330:974–80.
10. Van der Kamp MW, Mulholland AJ (2013) Combined quantum mechanics/molecular mechanics (QM/MM) methods in computational enzymology. *Biochemistry* 52:2708–28.
11. Sirin S, Pearlman D a, Sherman W (2014) Physics-based enzyme design: Predicting binding affinity and catalytic activity. *Proteins* 82:3397–409.
12. Yin S, Ding F, Dokholyan N V (2007) Eris: an automated estimator of protein stability. *Nat Methods* 4:466–7.
13. Yin S, Ding F, Dokholyan N V (2007) Modeling backbone flexibility improves protein stability estimation. *Structure* 15:1567–76.
14. Karginov A V, Ding F, Kota P, Dokholyan N V, Hahn KM (2010) Engineered allosteric activation of kinases in living cells. *Nat Biotechnol* 28:743–7.
15. Kota P et al. (2014) The N-terminal domain allosterically regulates cleavage and activation of the epithelial sodium channel. *J Biol Chem* 289:23029–42.
16. Proctor E a. et al. (2014) Rational coupled dynamics network manipulation rescues disease-relevant mutant cystic fibrosis transmembrane conductance regulator. *Chem Sci* 6:1237–1246.
17. Shirvanyants D, Ding F, Tsao D, Ramachandran S, Dokholyan N V (2012) Discrete Molecular Dynamics: An Efficient And Versatile Simulation Method For Fine Protein Characterization. *J Phys Chem B* 116:8375–8382.
18. Ding F, Tsao D, Nie H, Dokholyan N V (2008) Ab Initio Folding of Proteins with All-Atom Discrete Molecular Dynamics. *Structure* 16:1010–1018.
19. Dunbrack RL, Karplus M (1993) Backbone-dependent rotamer library for proteins. Application to side-chain prediction. *J Mol Biol* 230:543–74.
20. Yin S, Biedermannova L, Vondrasek J, Dokholyan N V (2008) MedusaScore: an accurate force field-based scoring function for virtual drug screening. *J Chem Inf Model* 48:1656–62.
21. Chodera JD, Swope WC, Pitera JW, Seok C, Dill K a. (2007) Use of the Weighted Histogram Analysis Method for the Analysis of Simulated and Parallel Tempering Simulations. *J Chem Theory Comput* 3:26–41.
22. Berendsen HJC, van der Spoel D, van Drunen R (1995) GROMACS: A message-passing parallel molecular dynamics implementation. *Comput Phys Commun* 91:43–56.
23. Pronk S et al. (2013) GROMACS 4.5: a high-throughput and highly parallel open source molecular simulation toolkit. *Bioinformatics* 29:845–54.
24. Schrödinger, LLC (2010) *The PyMOL Molecular Graphics System, Version~1.3r1*.

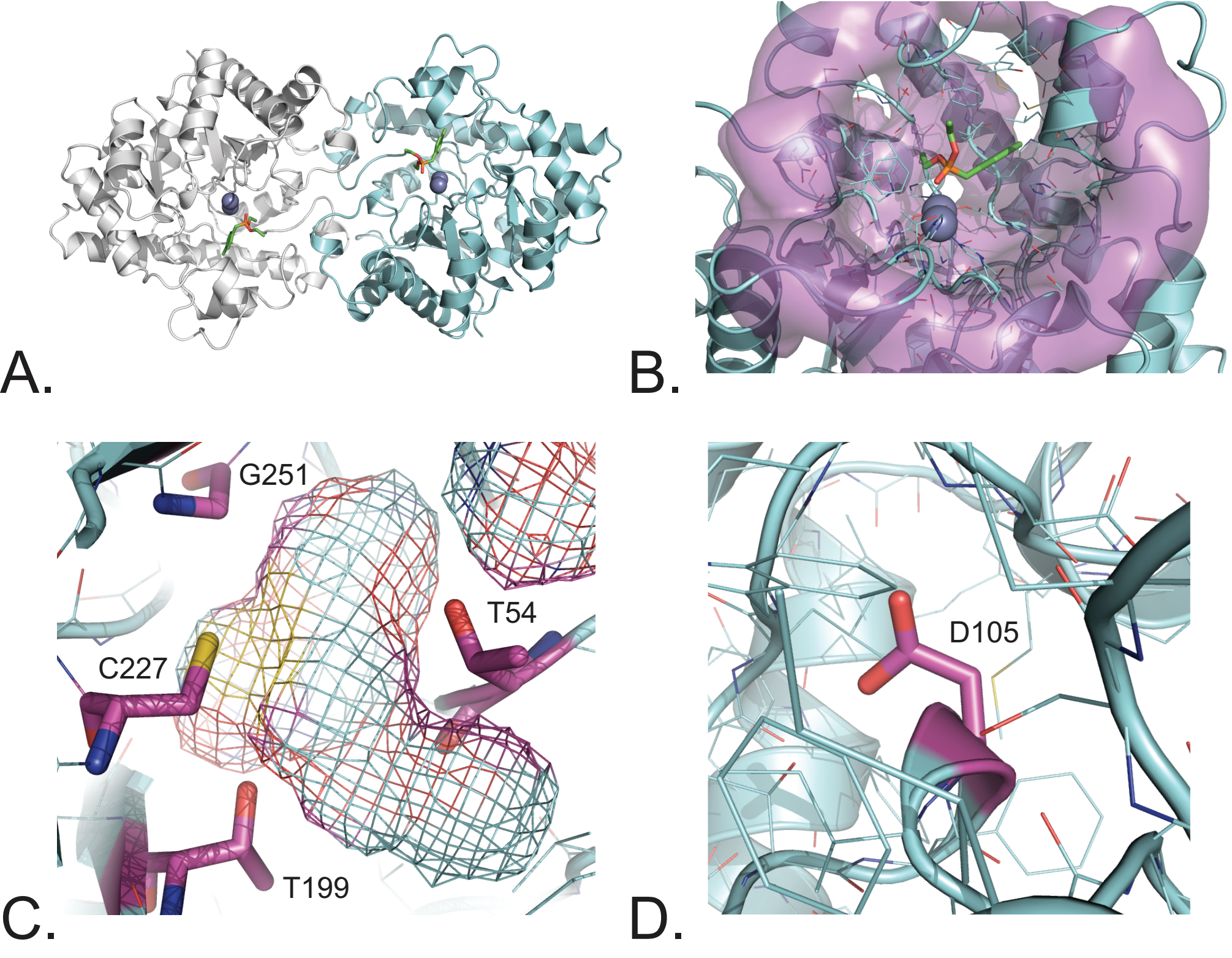
A.
B.
G251
T54
C227
T199
C.
D105
D.

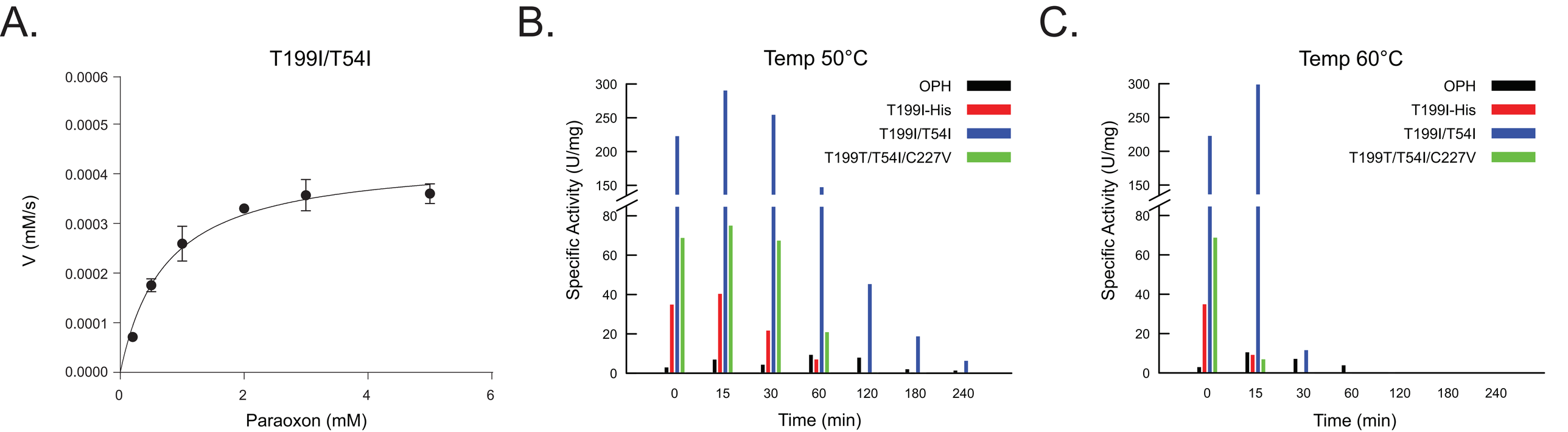
A.
T199I/T54I
V (mM/s)
0.0006
0.0005
0.0004
0.0003
0.0002
0.0001
0.0000
0
2
4
6
Paraoxon (mM)
B.
Temp 50°C
Specific Activity (U/mg)
300
250
200
150
80
60
40
20
0
OPH
T199I-His
T199I/T54I
T199T/T54I/C227V
0
15
30
60
120
180
240
Time (min)
C.
Temp 60°C
Specific Activity (U/mg)
300
250
200
150
80
60
40
20
0
OPH
T199I-His
T199I/T54I
T199T/T54I/C227V
0
15
30
60
120
180
240
Time (min)

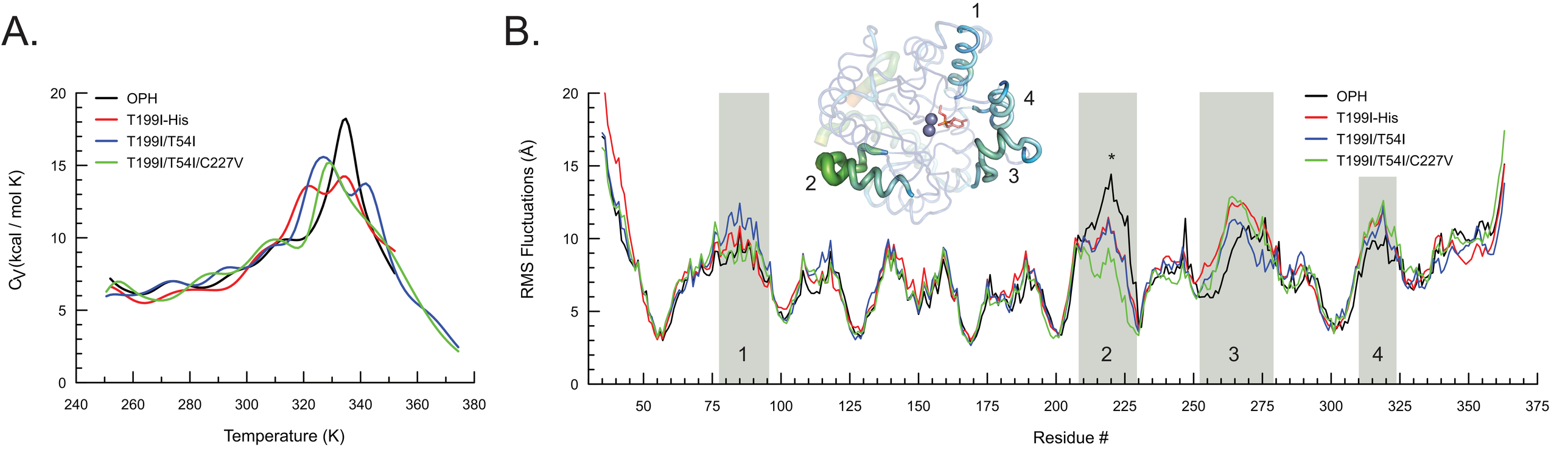
A.
B.
OPH
T199I-His
T199I/T54I
T199I/T54I/C227V
Cv (kcal / mol K)
Temperature (K)
RMS Fluctuations (Å)
Residue #
1
2
3
4
*

Purified OPH

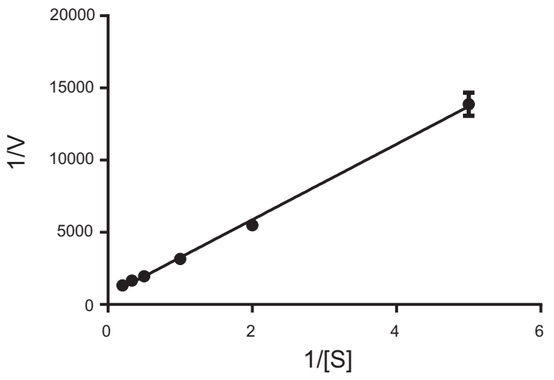

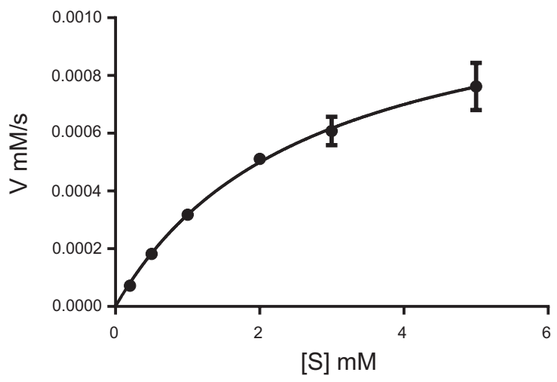

CFS-OPH

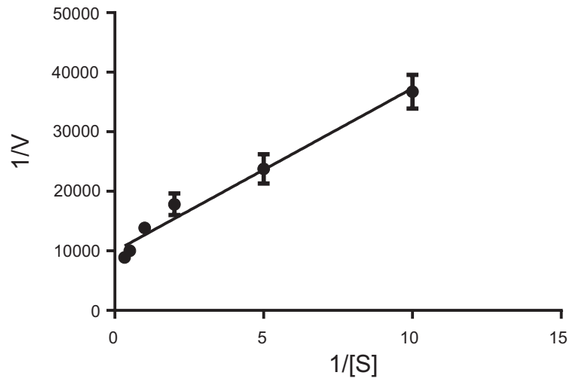

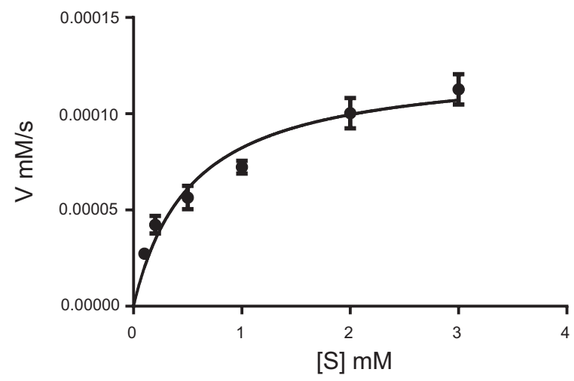

T54M

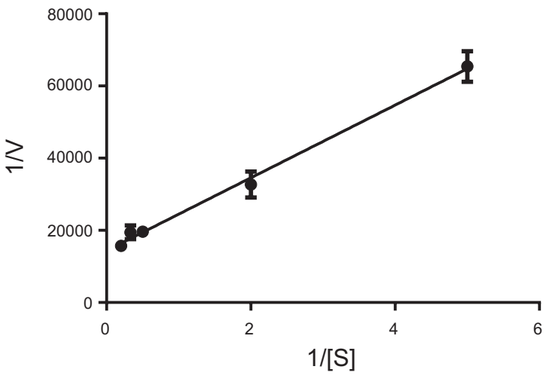

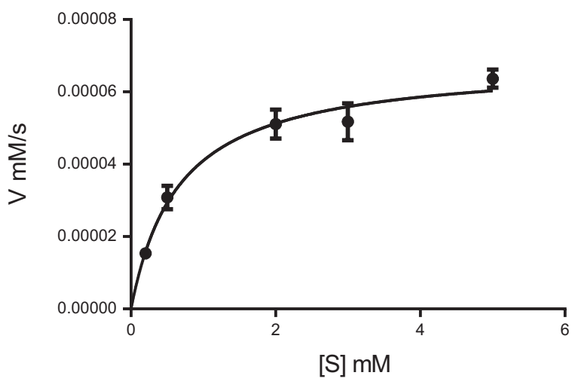

T199I-His

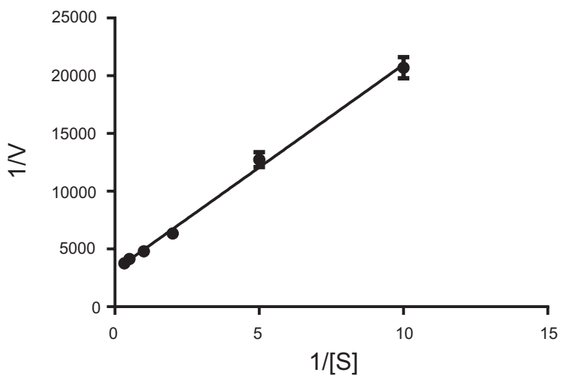

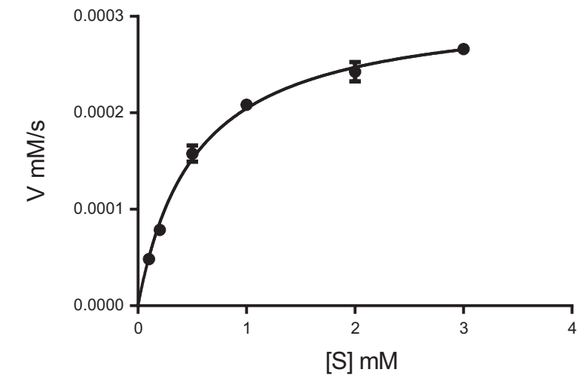

C227M-His

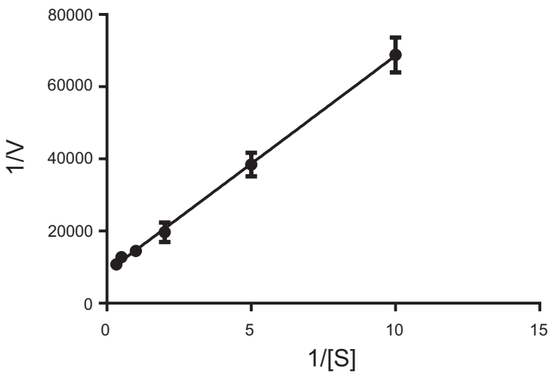

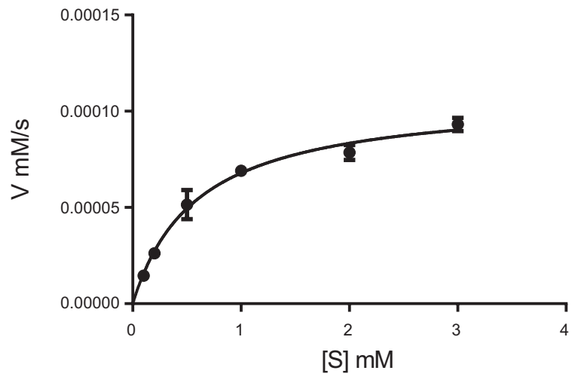

C227M/T54I-His

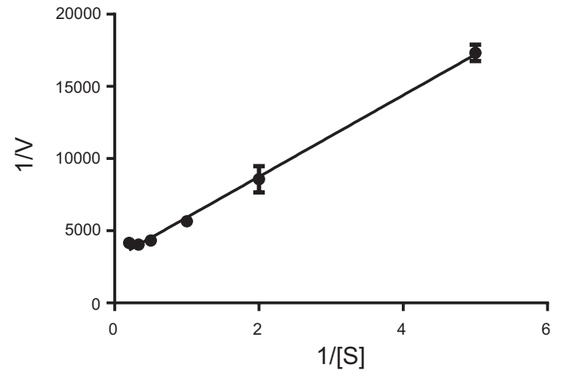

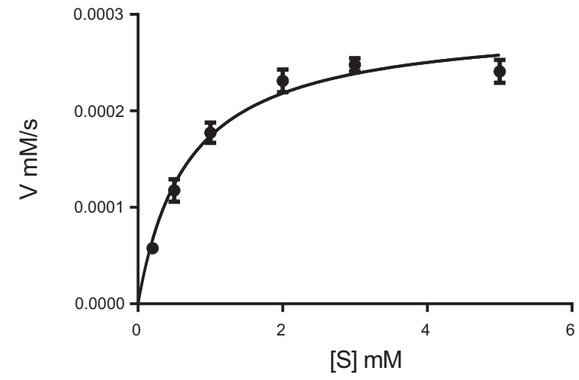

C227V/T54I-His

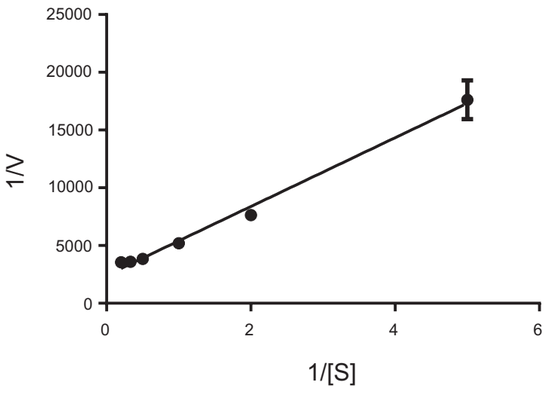

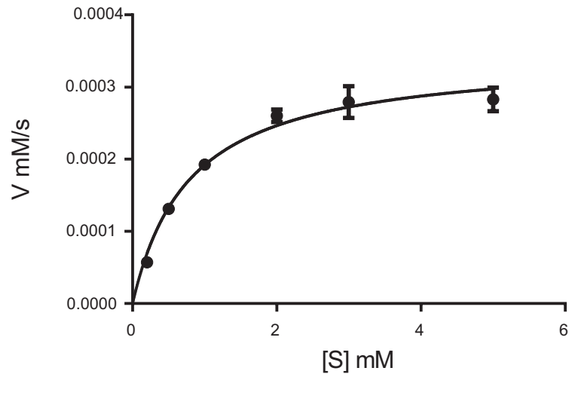

C227V/T199I-His

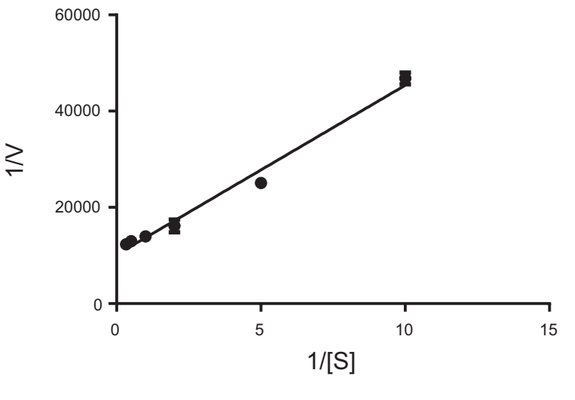

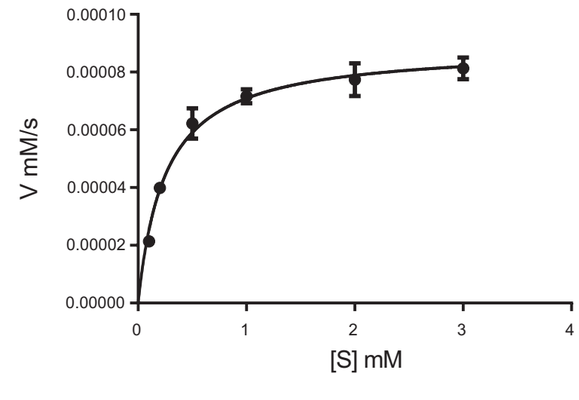

T199I/T54I-His

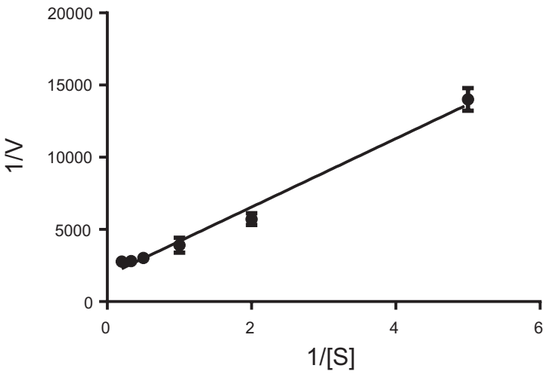

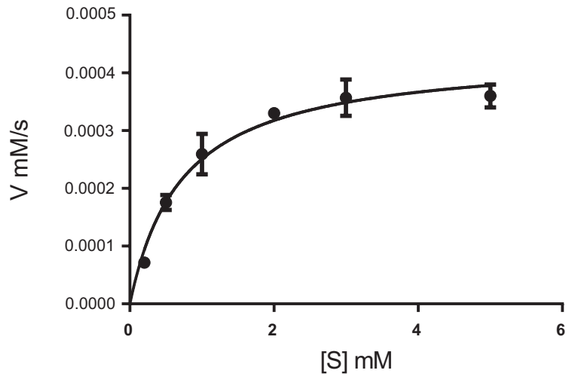

C227M/T199I-His

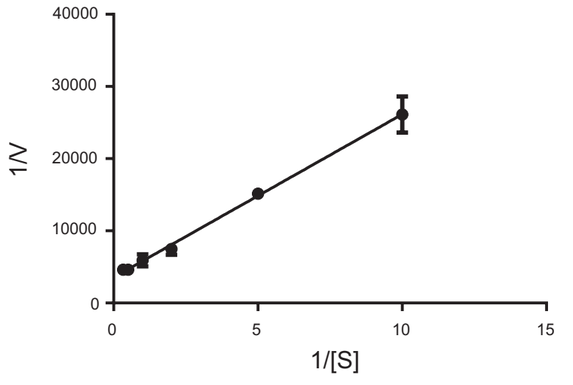

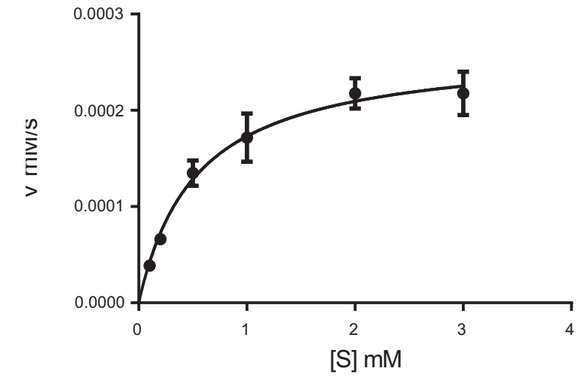

C227M/T54M-His

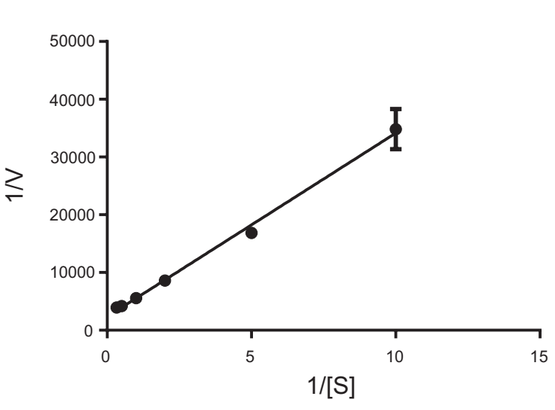

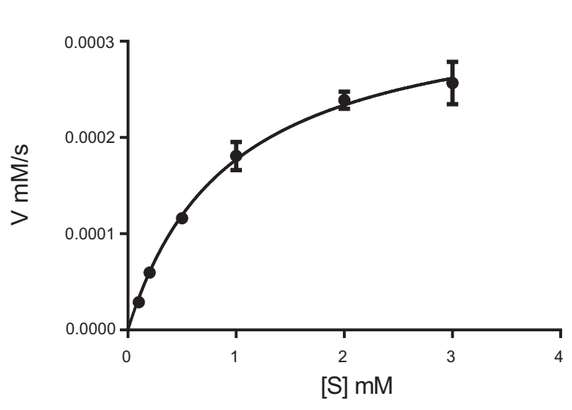

T199I/T54I/C227V-His

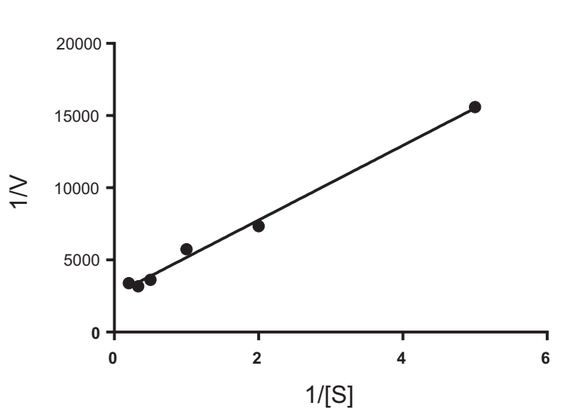

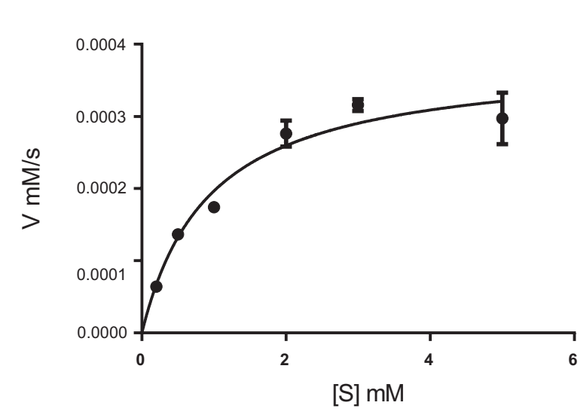

T199I/T54I/C227M-His

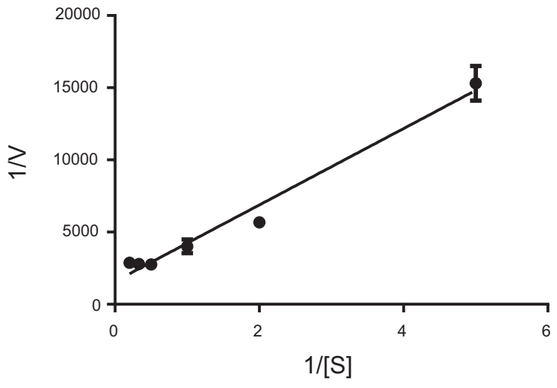

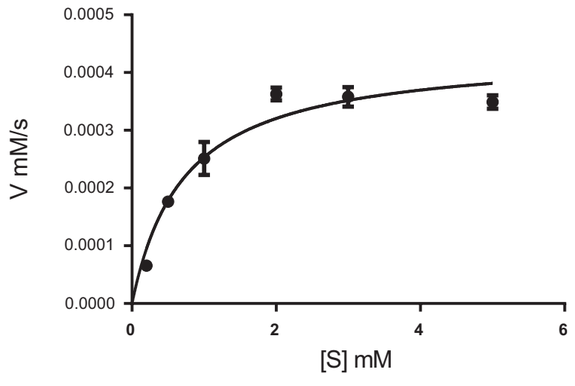

A. Single

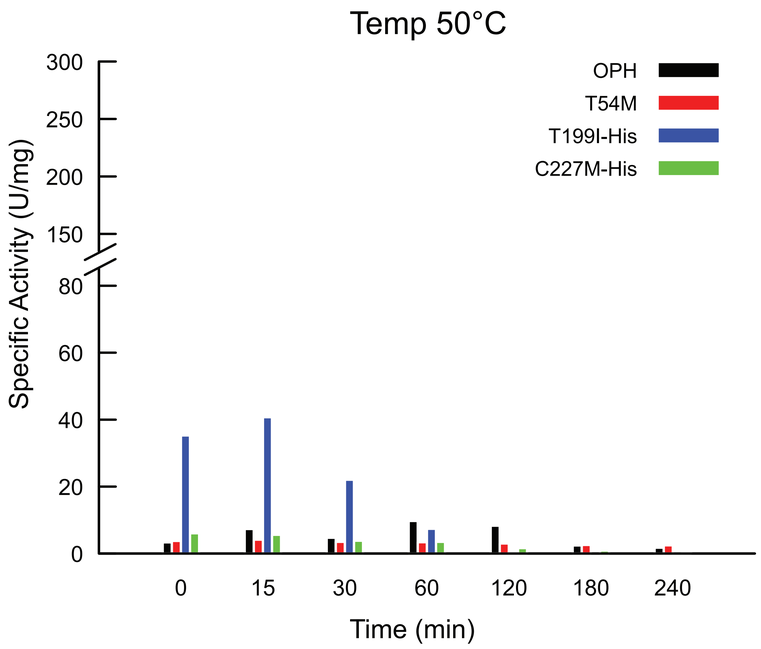

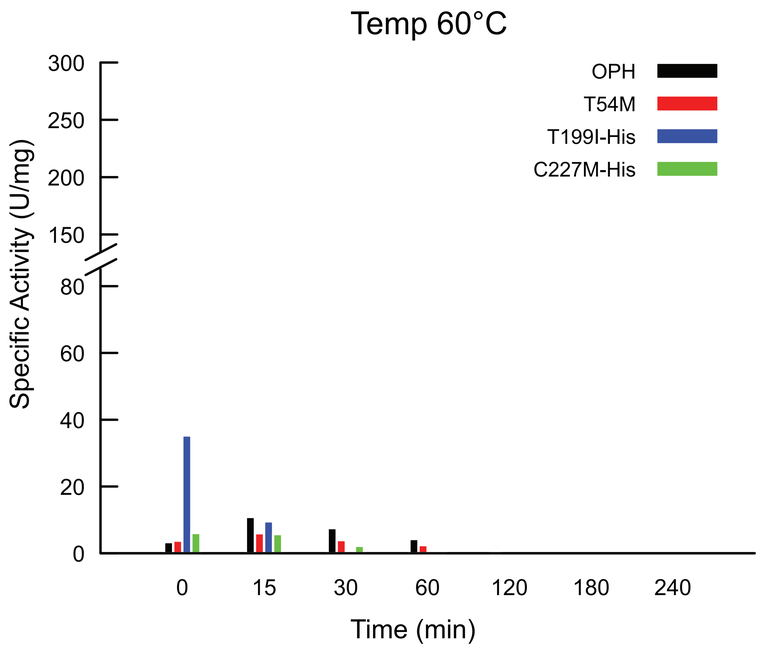

B. Double

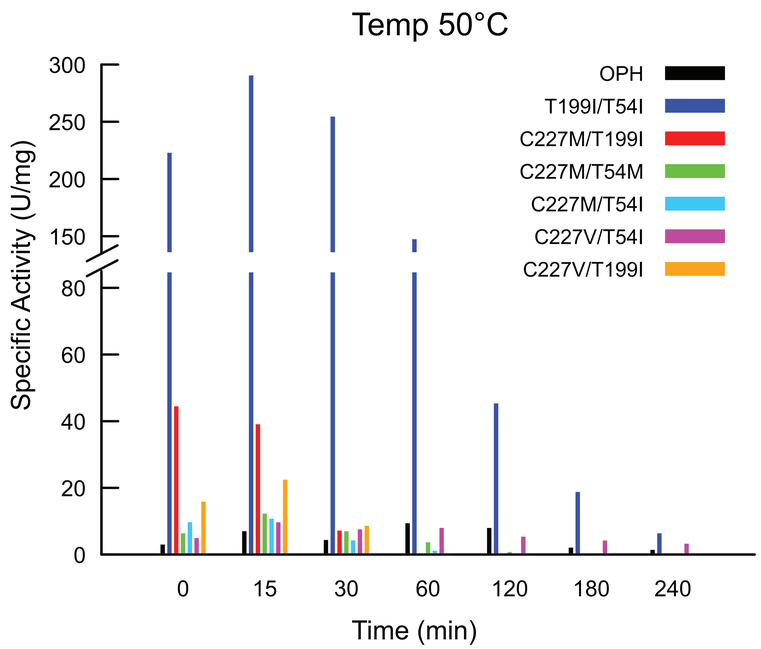

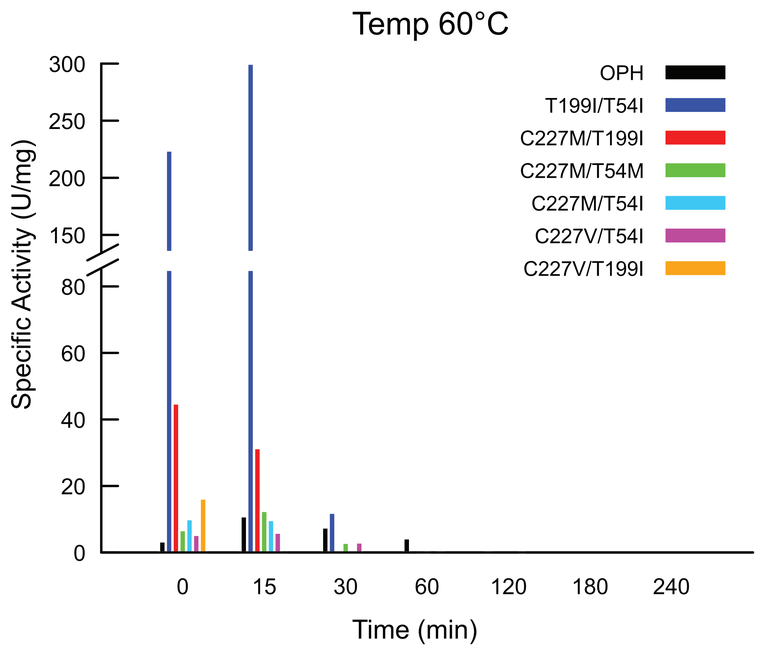

C. Triple

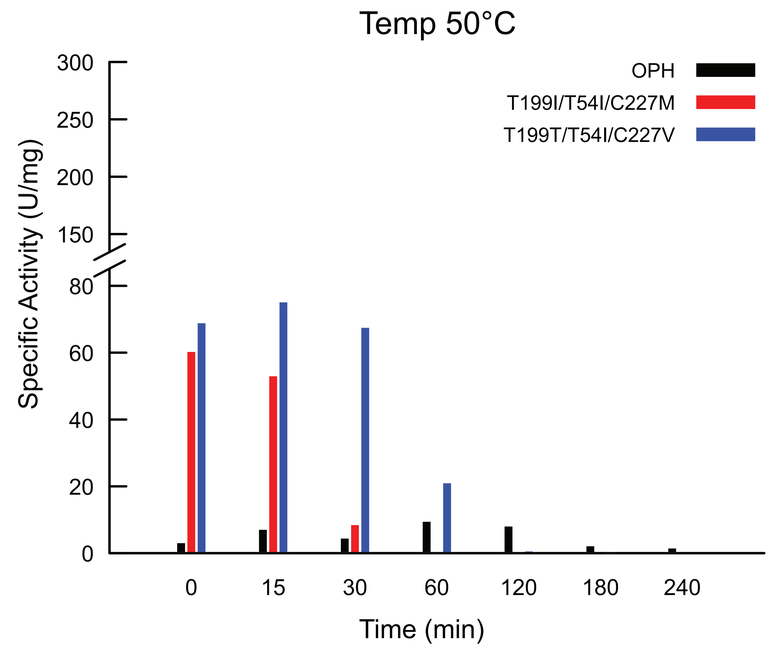

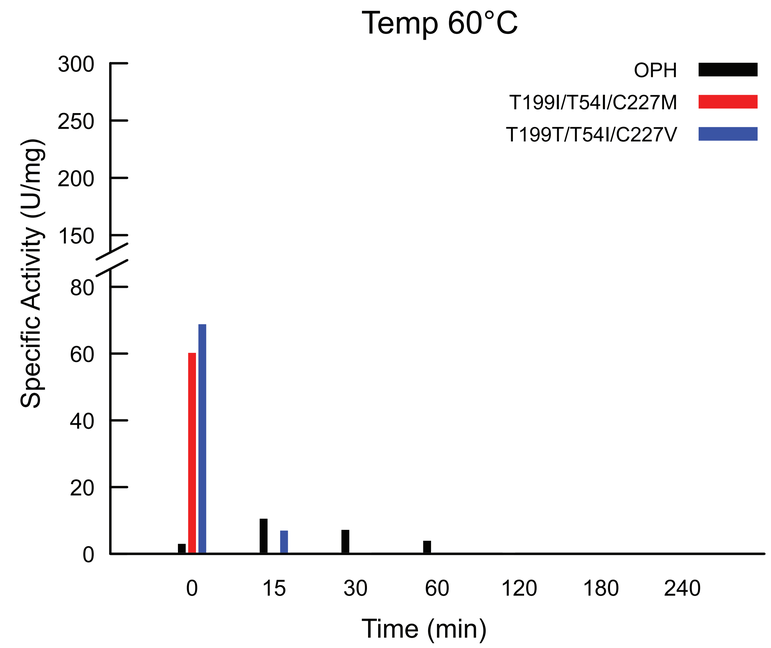

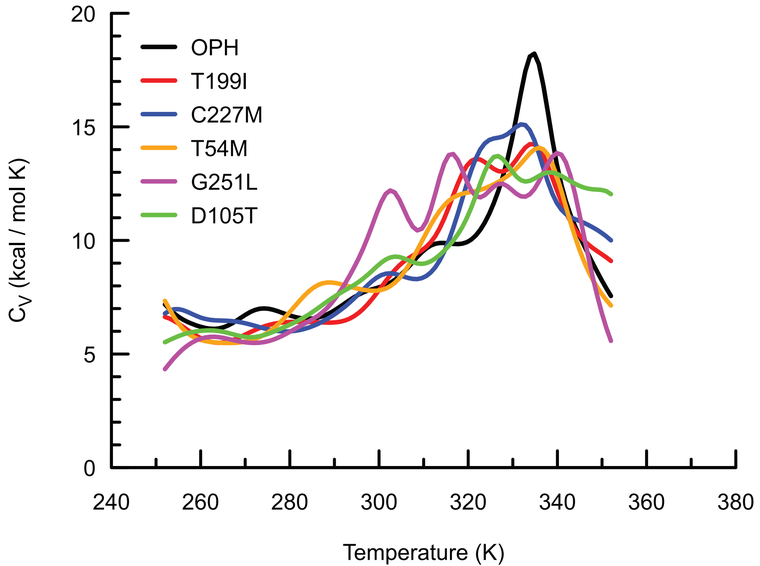

A. Single

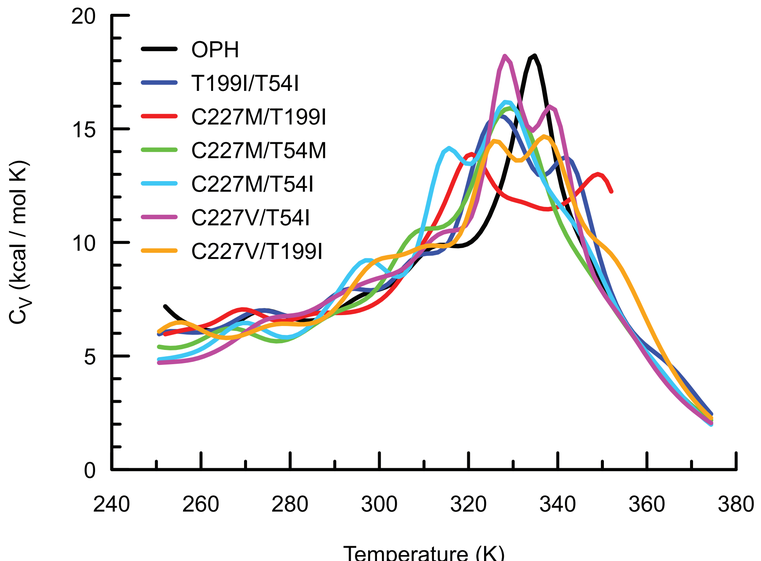

B. Double

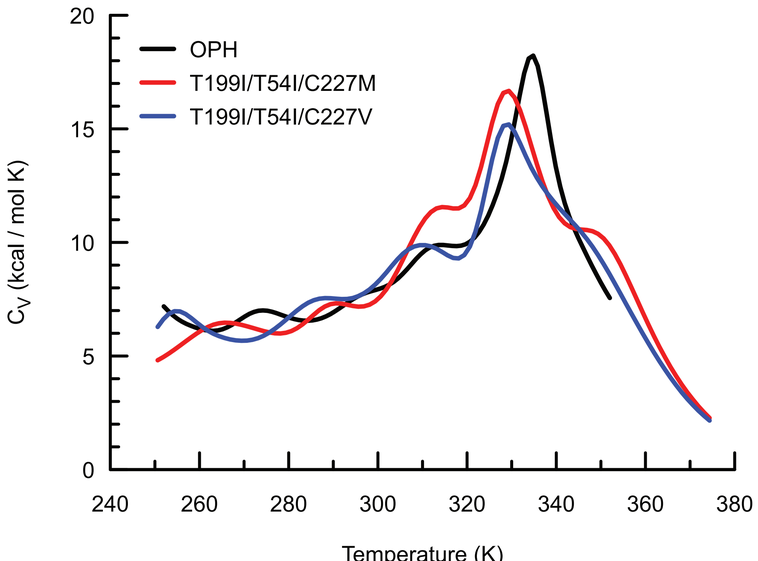

C. Triple

A. Single

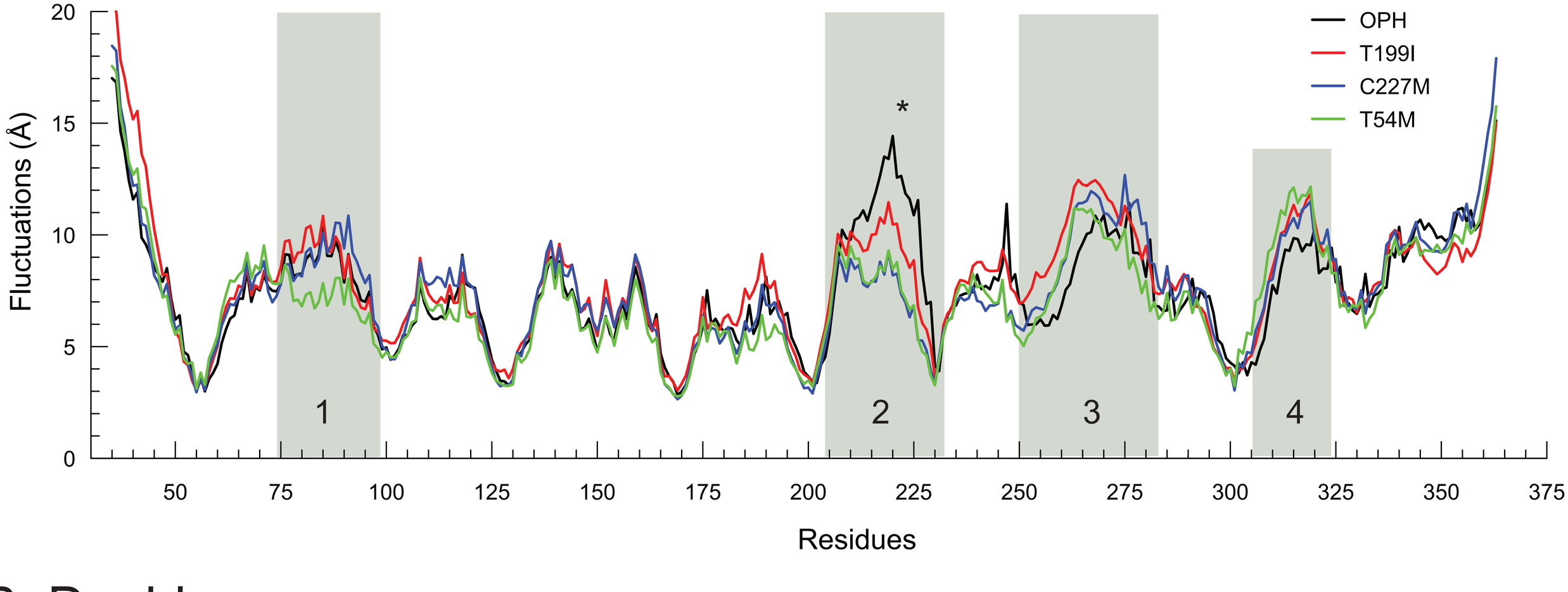

B. Double

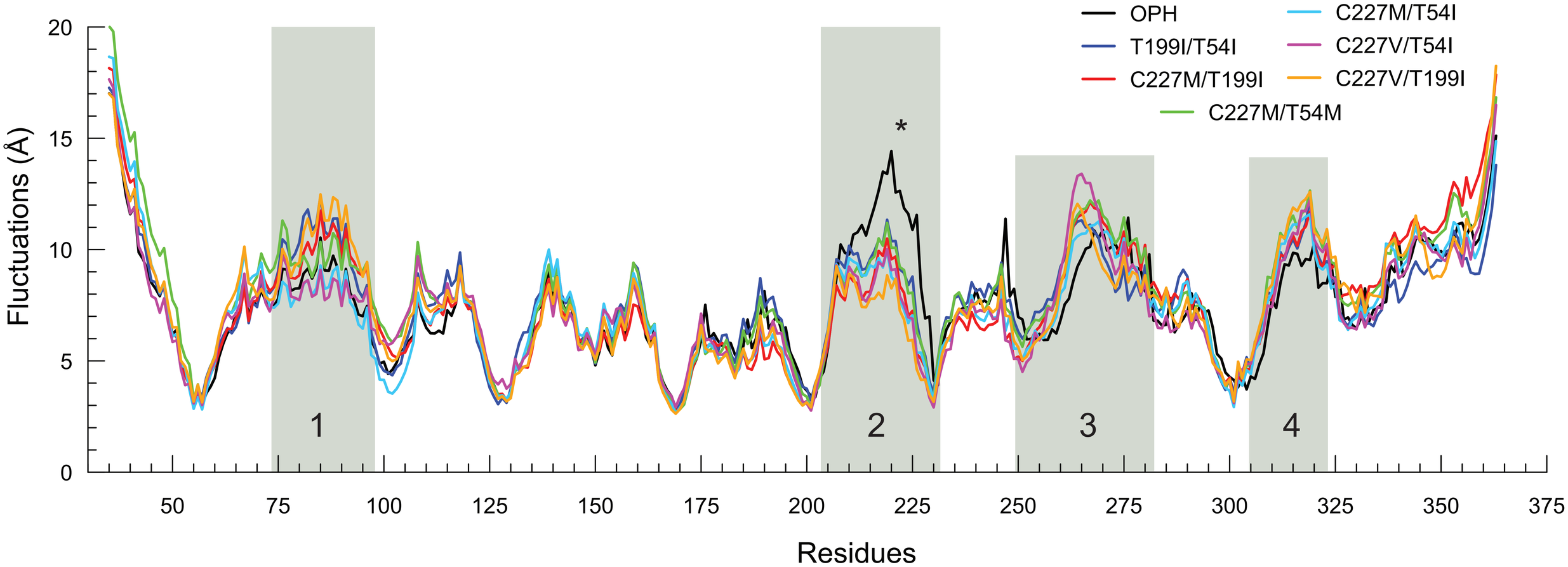

C. Triple

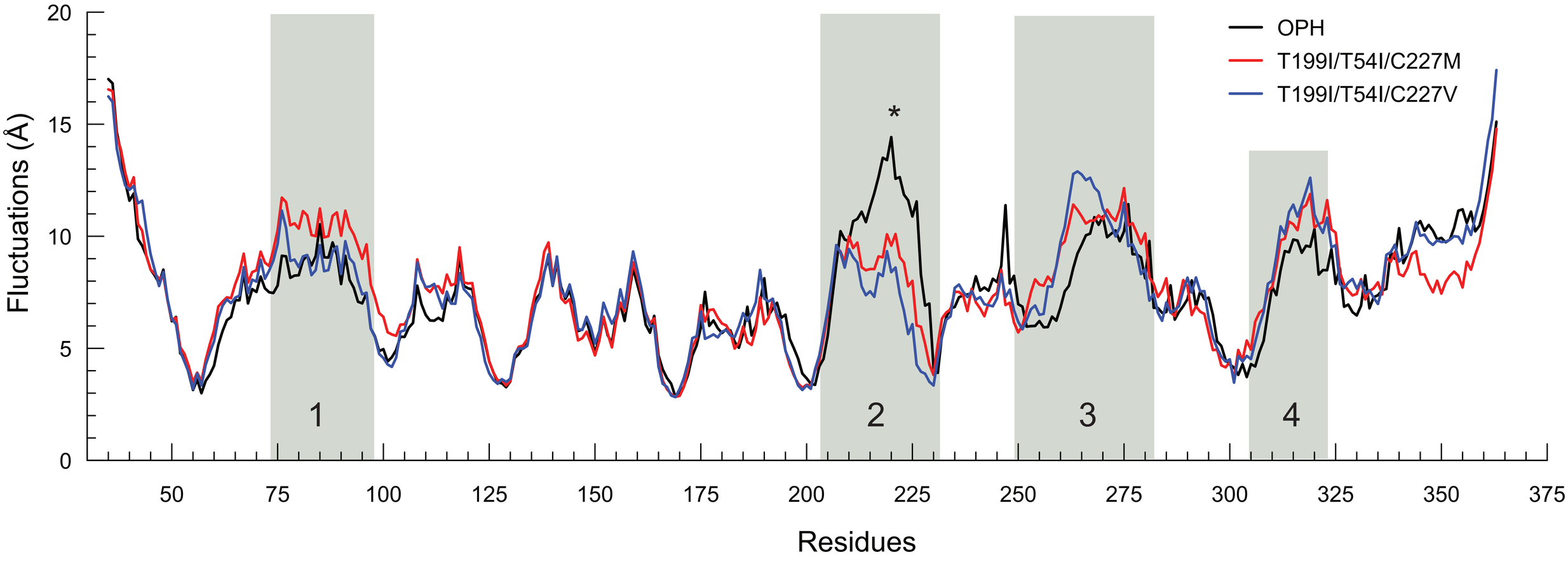

Figure Legends

Figure 1. Structural representations of OPH and identified mutation positions. A) Native homodimer structure of organophosphate hydrolase. Zinc ions shown as spheres with paraoxon ligand in stick figure (green). B) OPH monomer with the bound ligand (green), metal coordinated atoms (spheres), active site residues (lines), and the residues located between five and ten Å beyond zinc ions considered by the protein stability scan (highlighted in magenta). C) Hotspot results of residue positions G251, C227, T199, and T54 (magenta) surrounding an internal void shown in mesh surface. D) Residue position D105 (magenta) showing a buried unpaired polar amino acid. All structure figures created using Pymol (24).

Figure 2. Illustrative of experimental kinetic data performed at various temperatures. Panel A) an example of a standard Michealis-Menton kinetic plot of the activity of the double mutation T199I/T54I performed at room temperature. Panels B and C compare the best single mutation, T199I (red), double mutation T199I/T54I (blue), and triple mutation T199I/T54I/C227V (green), with wild-type OPH (black). Panel B shows the specific activity for these mutants performed at 50°C. Panel C shows the same mutations with the temperature raised to 60°C.

Figure 3. The analysis of computational simulations to understand the effect of mutations. Panels A and B compare the best single mutation, T199I (red), double mutation, T199I/T54I (blue), and triple mutation, T199I/T54I/C227V (green), with wild-type OPH (black). Panel A shows the reaction coordinate obtained from replica exchange DMD processed by WHAM. Panel B shows the root mean square fluctuation per residue over 1,000,000 time steps of equilibrium DMD simulations. Each mutation is an average of ten equilibrium DMD runs with a setting of 0.62 reduced temperature units. Highlighted segments represent those differences that have somewhat significant to significant values (p-value < 0.05 and < 0.01 respectively). Corresponding segments and fluctuations are mapped to the crystal structure (PDB Id 1DPM). The asterisk on segment 2 indicates a highly significant change across all mutation combinations.

Figure S1. Kinetic experimental data displayed as standard Michaelis-Menton and Lineweaver-Burke plots. Included is purified OPH, the cell free system OPH, and applicable single, double, and triple mutations.

Figure S2 – Increased temperature assays showing the experimental specific activity as observed for single (A), double (B), and triple (C) mutations. The upper graph is at 50°C with the lower at 60°C.

Figure S3 – Replica exchange DMD simulations with WHAM applied displaying calculated specific heat reaction coordinates for single (A), double (B) and triple (C) mutations.

Figure S4 – Root Mean Square Fluctuations observed from an average of ten equilibrium DMD runs per mutation at a reduced temperature of 0.62. Panel A) single mutations, B) double mutations and C) triple mutations.